Simulation of Layer-By-Layer Toner Deposition from a Uniform Toner Cloud in Gap-Jump Monocomponent Development Systems With an AC Developer Bias

Jang Yi and Richard B. Wells

MRC Institute, University of Idaho, Moscow, Idaho, USA

Time dependent layer-by-layer toner development in AC biased monocomponent systems is numerically simulated. For a given gap length, a uniform toner cloud is assumed to be formed in the gap prior to initial development. The normal electric field in the toner cloud is obtained by taking the two-dimensional Fourier transform of the spatial potential and subsequently taking the negative gradient of the potential. The field is then used to determine the locations of toner deposition in each toner layer, whose thickness is obtained from the average toner particle size. As the photoconductor (PC) rolls away from the developer, the effective gap length increases and the sinusoidal AC bias oscillates. The time dependent effective gap length as a function of PC rotation angle is calculated using conformal mapping techniques. Our development calculation is carried out iteratively until the developed layers from the positive and negative peaks of the AC bias stabilize. Simulation results using different input bitmaps are presented and analyzed.

Journal of Imaging Science and Technology 48: 324–334 (2004)

Introduction

Electrophotographic printers have become indispensable to the modern office and now constitute a multi-billion dollar industry involving many of the world's largest corporations.[1] The most crucial part of the electrophotographic process, which is not well understood, is the development step because this step most directly determines the quality of the images. Many approaches have been reported for predicting the outputs of electrophotographic devices in terms of optical density/gray level,[2–6] developed toner mass,[1,7–9] and electric field.[10–14] In this article, we introduce a procedure for calculating developed toner layers while dynamically accounting for the effects of AC bias.

Accurately determining the amount of developed toner requires knowledge of the total forces acting on toner particles in the gap, which are quite complicated. In addition to the development field, a first principles treatment would need to account for other forces acting on toner. Calculations attempting to account for these factors quickly become quite involved.[15,16] AC biased development systems pose an even more formidable challenge since toner particles bounce back and forth between the developer roller and photoconductor (PC) multiple times in such systems, and accounting for the time dependent dynamics is very difficult.[2] In this article, such dynamic behavior is simulated by using the negative and positive peaks of the AC bias and accurately increasing the gap length accordingly. This approach is based on uniform toner distribution in the gap and the polarity of the normal field determines the direction, in which toner particles travel.

For more consistent and reliable outputs from a laser printer, it is a common practice to apply an AC bias to the developer. Since the magnitude of a typical AC bias is in the neighborhood of 2000 Vp-p (peak-to-peak voltage), the final development depends heavily on how the electric field changes as the PC rolls away from the developer. We will first calculate the effective gap length as a function of PC rotation angle using conformal mapping techniques. The frequency of the AC bias specifies how long it takes for the AC bias to change its polarity. The PC rotation angle immediately after the AC bias switches its polarity can be determined from the geometry. We then derive the normal field expression in the gap using the effective gap length and describe our layer-by-layer development method, which takes into account the time dependent AC bias.

It should be mentioned that our simulation is based on the assumption that the electric forces in the gap predominantly determines the final outcome. In the presence of other forces, it can be expected that the final PC rotation angle in our development model will be different from that which occurs in the actual system

Original manuscript received April 8, 2003

yi9534@uidaho.edu; phone: 208-885-9718; fax: 208-885-6840: rwells@uidaho.edu; phone: 208-885-4353; fax: 208-885-6840

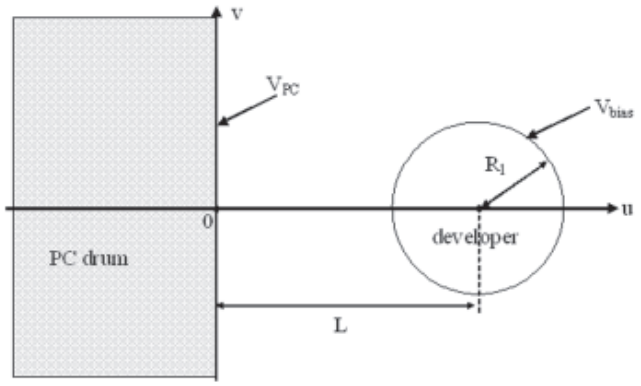

Figure 1. w coordinate system (flat PC)

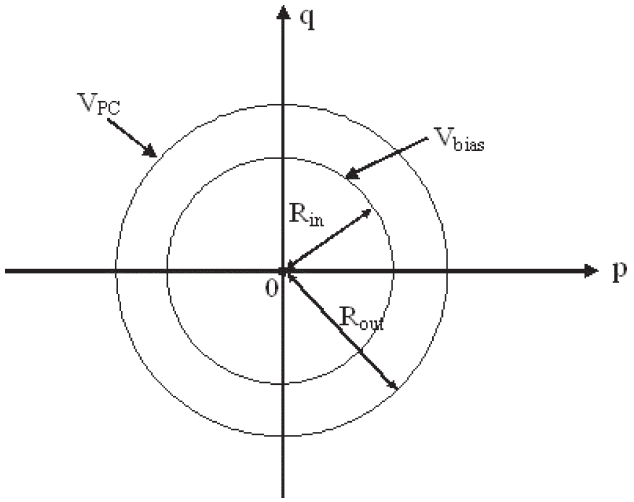

Figure 2. r coordinate system

(more comprehensive characterization of the gap jump development process including the effects from other forces is a topic of future research). For example, surface adhesion will require a more normal electric field to detach toner layers from the developer and PC, which will effectively reduce the final development angle. However, in other aspects the dynamics reported in this article should be representative of the development process.

Flat PC and Cylindrical Developer

Suppose the PC radius is much greater than the developer radius. Then we can assume that the PC surface is flat, as illustrated in Fig. 1. We map the region between the PC and developer onto the annular region between two circles of radii, R_{out} and R_{in}, as shown in Fig. 2 using the following bilinear transformation

$$\mathbf{r} = \frac{a_1\mathbf{w} + b_1}{c_1\mathbf{w} + d_1} \quad \leftrightarrow \mathbf{w} = \frac{-d_1\mathbf{r} + b_1}{c_1\mathbf{r} - a_1}, \tag{1}$$

where the coordinate system of the developer and flat PC is given by

$$\mathbf{w} = u + iv, \tag{2}$$

and the coordinate system of the annulus is given by

$$\mathbf{r} = p + iq. \tag{3}$$

The circle in the (u, v) coordinate system is mapped onto the inner circle of the annulus in Fig. 2 and the v-axis is mapped onto the outer circle of the annulus. With these two constraints, we let $R_{in} = c_1 = 1$ and obtain

$$\begin{aligned} R_{in} &= 1 \\ R_{out}^2 &= \frac{L^2 - R_1^2 + L\sqrt{L^2 - R_1^2}}{-L^2 + R_1^2 + L\sqrt{L^2 - R_1^2}} \\ c_1 &= 1 \\ a_1 &= R_{out} \\ d_1 &= \sqrt{L^2 - R_1^2} \\ b_1 &= -R_{out}\sqrt{L^2 - R_1^2} \end{aligned} \quad . \tag{4}$$

It can be shown that the potential inside the annulus is[17]

$$V(p,q) = V_{dev} + \frac{V_{PC} - V_{dev}}{\ln R_{out}} \ln|p + iq|. \tag{5}$$

From Eq. (1),

$$V(u,v) = V_{dev} + \frac{V_{PC} - V_{dev}}{\ln R_{out}} \ln\left|\frac{a_1\mathbf{w} + b_1}{c_1\mathbf{w} + d_1}\right|. \tag{6}$$

In order to determine the locations of field lines, along which toner particles will travel, we need to obtain the harmonic conjugate of Eq. (6). The harmonic conjugate $\tilde{V}(u,v)$ must satisfy the following Cauchy–Riemann equations,

$$\begin{aligned} \frac{\partial}{du} V(u,v) &= \frac{\partial}{dv} \tilde{V}(u,v) \\ \frac{\partial}{dv} V(u,v) &= -\frac{\partial}{du} \tilde{V}(u,v) \end{aligned}. \tag{7}$$

Integrating the both sides of the first Cauchy–Riemann equation and taking advantage of the second Cauchy–Riemann equation, we obtain

$$\tilde{V}(u,v) = \frac{V_{PC} - V_{dev}}{\ln R_{out}} \left[\arctan\left(\frac{v}{u + b_1/a_1}\right) - \arctan\left(\frac{v}{u + d_1/c_1}\right)\right] + Q_0 \tag{8}$$

Cylindrical PC and Developer

In practice, the PC radius is not much larger than the developer radius (typically twice as large). Thus, the flat PC approximation is in general not valid. In order to incorporate a cylindrical PC (see Fig. 3), we introduce another bilinear mapping.

$$\mathbf{w} = \frac{a_0\mathbf{z} + b_0}{c_0\mathbf{z} + d_0} \quad \leftrightarrow \mathbf{z} = \frac{-d_0\mathbf{w} + b_0}{c_0\mathbf{w} - a_0}, \tag{9}$$

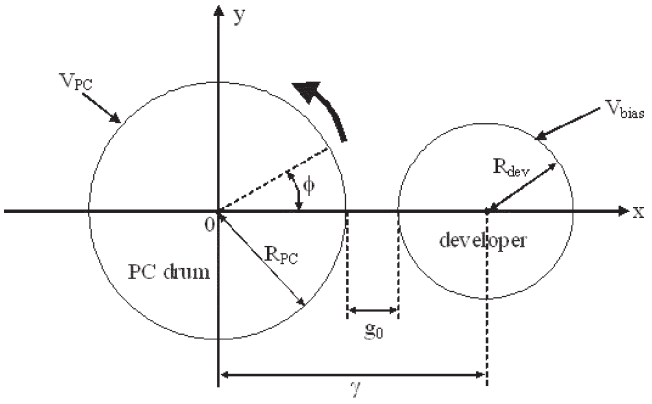

Figure 3. z coordinate system (cylindrical PC)

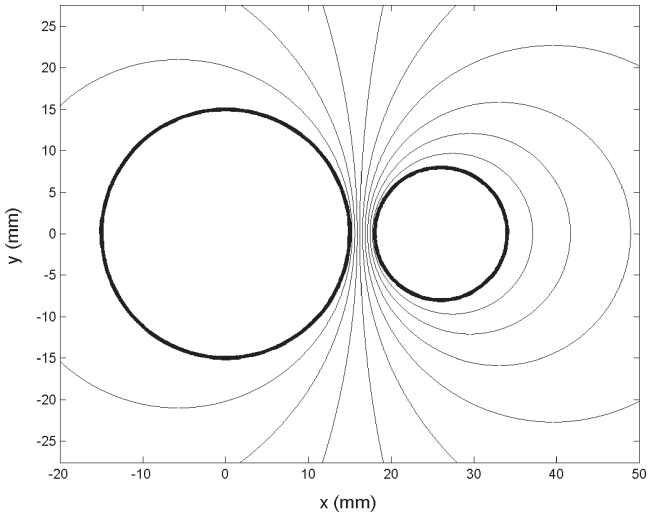

Figure 4. Equipotential curves

where the coordinate system of the cylindrical PC and developer is given by

$$\mathbf{z} = x + iy \tag{10}$$

Then, as similarly done in the flat PC case, we obtain

$$\begin{aligned} L &= \frac{\gamma^2 - R_{PC}^2 - R_{dev}^2}{R_{PC}^2 + \gamma^2 + 2\gamma R_{PC} - R_{dev}^2} \\ R_1^2 &= \frac{-R_{PC}^2 - \gamma^2 + 2\gamma R_{PC} + R_{dev}^2}{R_{PC}^2 + \gamma^2 + 2\gamma R_{PC} - R_{dev}^2} + L^2 \\ c_0 &= -1 \\ a_0 &= -1 \\ d_0 &= -R_{PC} \\ b_0 &= R_{PC} \end{aligned}, \tag{11}$$

where $\gamma = R_{PC} + g_0 + R_{dev}$. The two bilinear transformations of Eqs. (1) and (9) can be combined to yield one composite mapping

$$\mathbf{r} = \frac{a\mathbf{z} + b}{c\mathbf{z} + d} \quad \leftrightarrow \mathbf{z} = \frac{-d\mathbf{r} + b}{c\mathbf{r} - a}, \tag{12}$$

where

$$\begin{aligned} a &= a_0 a_1 + b_1 c_0 \\ b &= a_1 b_0 + b_1 d_0 \\ c &= a_0 c_1 + c_0 d_1 \\ d &= b_0 c_1 + d_0 d_1 \end{aligned}. \tag{13}$$

With this new mapping, we can directly map the gap in Fig. 3 onto the region inside the annulus in Fig. 2. From Eq. (6),

$$V(x,y) = V_{dev} + \frac{V_{PC} - V_{dev}}{\ln R_{out}} \ln\left|\frac{a\mathbf{z} + b}{c\mathbf{z} + d}\right|. \tag{14}$$

As derived earlier, the harmonic conjugate of Eq. (14) is

$$\tilde{V}(x,y) = \frac{V_{PC} - V_{dev}}{\ln R_{out}}\left[\arctan\left(\frac{y}{x + b/a}\right) - \arctan\left(\frac{y}{x + d/c}\right)\right] + Q_1. \tag{15}$$

The equipotential curves are given by

$$V(x,y) = V_0. \tag{16}$$

The equipotential curves using several values of V_0 are shown in Fig. 4. Equation (16) turns out to be the equation of circles with different radii and centers that vary with V_0. Thus we can analytically obtain the length of a portion of an equipotential curve once we know its curvature. However, the lines of flux given by

$$\tilde{V}(x,y) = E_0 \tag{17}$$

are not easily expressed in terms of x and y. We note that the lines of flux in the (p, q) coordinate system are portions of rays emanating from the origin. Thus, if we use the polar coordinate system, a line of flux inside the annulus can be expressed as

$$\mathbf{r} = R\cos\theta + iR\sin\theta, \tag{18}$$

where

$$R_{in} \le R \le R_{out}, \tag{19}$$

and θ is the angle of the flux line with respect to the positive x-axis. Then from Eqs. (18) and (12),

$$x(R) = \frac{-cdR^2 + (bc + ad)R\cos\theta - ab}{c^2R^2 - 2acR\cos\theta + a^2}, \tag{20}$$

and

$$y(R) = \frac{(ad - bc)R\sin\theta}{c^2R^2 - 2acR\cos\theta + a^2}. \tag{21}$$

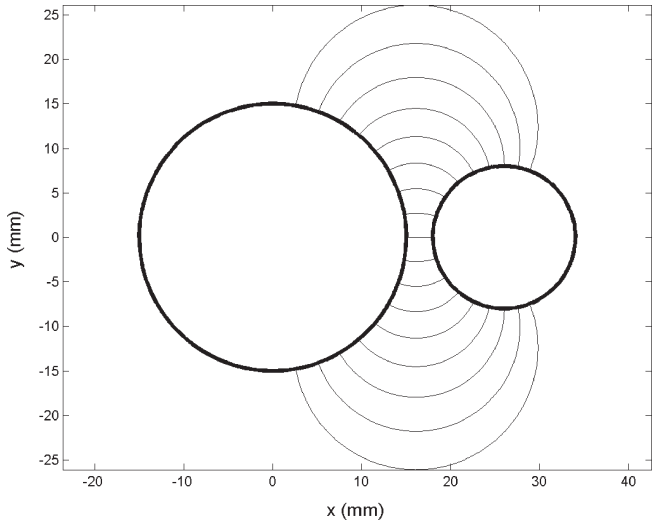

Figure 5. Lines of flux

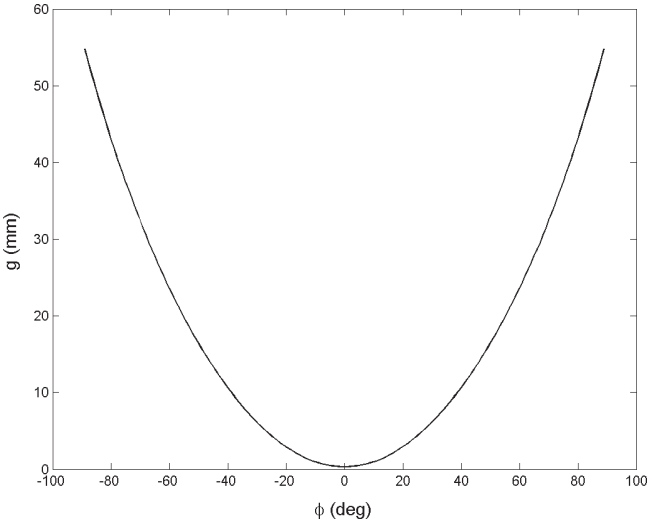

Figure 6. Lengths of flux lines

Given a PC rotation angle ϕ, we can obtain the x and y positions on the PC surface. Then

$$\theta = \frac{\mathrm{Im}\left\{\dfrac{a(x+iy)+b}{c(x+iy)+d}\right\}}{\mathrm{Re}\left\{\dfrac{a(x+iy)+b}{c(x+iy)+d}\right\}}. \tag{22}$$

Thus, for an arbitrary ϕ, Eqs. (20) and (21) represent the corresponding flux line. Figure 5 shows the flux lines resulting from $\phi = \{-80°, -70°, -60°, \ldots, 60°, 70°, 80°\}$.

The length g of a flux line is given by

$$g = \int_{R_{in}}^{Rout} \sqrt{\left(\frac{dx(R)}{dR}\right)^2 + \left(\frac{dy(R)}{dR}\right)^2}\, dR$$

$$= \frac{ad-bc}{|ac\sin\theta|}\left[\arctan\left(\frac{c^2 R_{out} - ac\cos\theta}{|ac\sin\theta|}\right) - \arctan\left(\frac{c^2 R_{in} - ac\cos\theta}{|ac\sin\theta|}\right)\right]. \tag{23}$$

This is the effective gap length for a given θ. The lengths of flux lines as a function of PC rotation angle ϕ are shown in Fig. 6.

Electric Field in the Gap

Consider the development region geometry shown in Fig. 7. Initially, when there is no toner on the PC (k = 0 in Fig. 7), we assume uniform toner distribution in the gap with a volume charge density of

$$\rho_{cloud} = \rho_t \frac{\lambda}{g}, \tag{24}$$

where ρ_t is the toner volume charge density, λ is the initial bead layer thickness, and g is the effective gap length in Eq. (23). In this case of no development, the

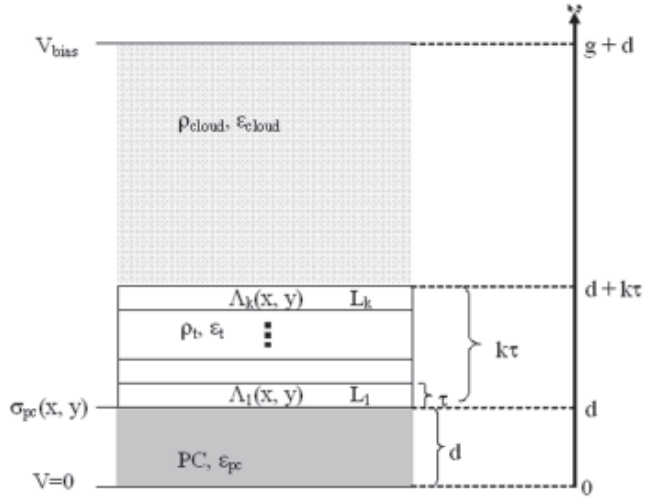

Figure 7. Development region geometry

field at the PC surface determines the development area on the PC surface. After the first layer, L_1 develops on the PC surface, k = 1 and the volume charge density above L_1 is reduced according to

$$\rho_{cloud} = \rho_t \frac{(\lambda - \tau)}{g}, \tag{25}$$

where τ is the thickness of each toner layer. We discretize the toner layer thickness in each layer based on our measurement of the average toner particle size. From τ, we can obtain the maximum number N of toner layers that can develop on the PC

$$N = \frac{\lambda}{\tau}, \tag{26}$$

After L_1 develops on the PC, the field on top of L_1 determines where on the PC the second layer, L_2, will develop. This process is repeated until ρ_{cloud} becomes zero,

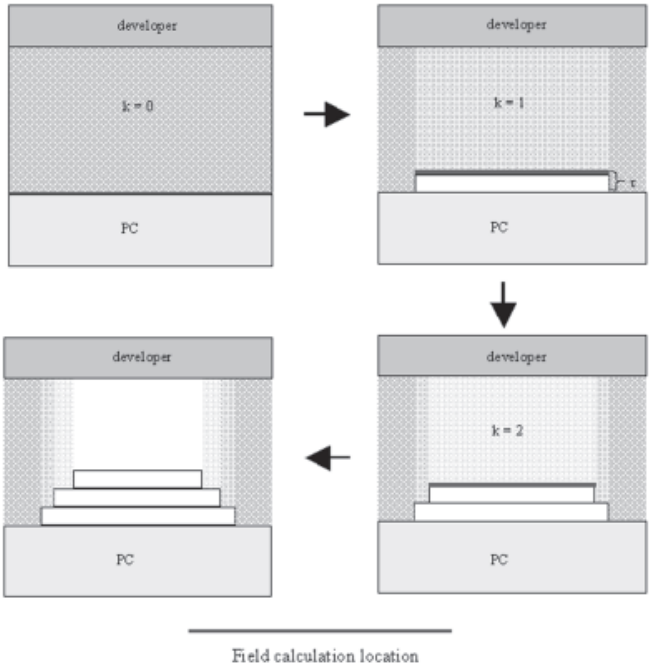

Figure 8. Layer-by-layer development. ρ_{cloud} varies with horizontal location

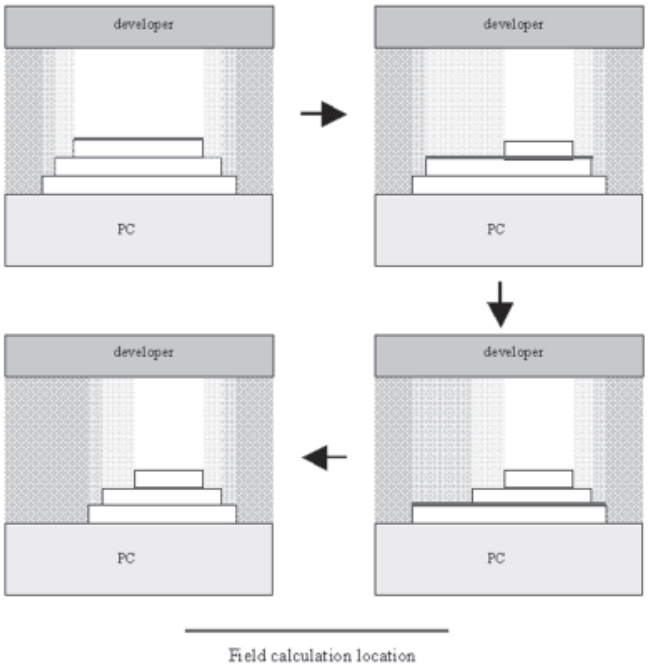

Figure 9. Toner removal process. ρ_{cloud} varies with horizontal location

or the field at the top of L_k is less than or equal to zero (negative field means the toner experiences a force which is directed upward towards the developer), which ever occurs first. Figure 8 illustrates this process for $N = 3$. Note that this process is valid for the negative peak of the AC bias (with negatively charged toner and PC). When the AC bias switches its polarity and reaches the positive peak, the toner particles will travel in the opposite direction (towards the developer). In this case, we calculate the field at the top of L_N (ρ_{cloud} above L_N is zero) and "undeveloped" portions of L_N where the field is negative. The removed portions of L_N effectively increases the volume charge density in the gap (directly above the removed toner) to

$$\rho_{cloud} = \rho_t \frac{\tau}{g}, \tag{27}$$

Once L_N is removed at appropriate locations, the field at the top of L_{N-1} determines which portions of L_{N-1} will be removed. This process is repeated until appropriate portions of L_1 are removed. This toner removal process is illustrated in Fig. 9, where toner removal takes place on the left side only for the purpose of illustration.

With our layer-by-layer development process described above, we now derive an expression for the normal field in the gap. Our derivation is carried out in the frequency domain, as similarly done by Kao.[13] For an arbitrary pattern, the development region is not known in advance, so it has to be a function of the spatial variables, x, and y. For the development at the PC, let

$$\Lambda_n(x,y) = \begin{cases} 1, & \text{toner at } (x,y,z = d + (n-1)\tau) \\ 0, & \text{no toner at } (x,y,z = d + (n-1)\tau) \end{cases} \quad 1 \le n \le N. \tag{28}$$

Thus, $\Lambda_3(x_0,y_0) = 1$ would mean that the third toner layer develops at (x_0,y_0) on the PC (see Fig. 7). Also, define

$$\Phi_n(x,y) = \begin{cases} 1, & if \quad \sum_{k=1}^{N} \Lambda_k(x,y) = n \\ 0, & else \end{cases} \quad 0 \le n \le N. \tag{29}$$

Then, the volume charge density in the gap can be written as

$$\rho_{cloud}(x,y,z) = \sum_{k=1}^{N} \rho_t \frac{\lambda - n\tau}{g} \Phi_k(x,y)\left[u\left(z-(d+n\tau)\right) - u\left(z-(d+g)\right)\right], \tag{30}$$

where $u(\cdot)$ is the unit step function. With the definitions, Eqs. (28) through (30), we begin with Poisson's equation in the frequency domain.

$$\left(\frac{\partial^2}{\partial z^2} - k_u^2\right) V(k_u,z) = -\frac{\rho_t}{\varepsilon_0 \varepsilon_t} \sum_{n=1}^{N} \Lambda_n(k_u)\left\{u\left[z-(d+(n-1)\tau)\right] - u\left[z-(d+n\tau)\right]\right\} - \frac{\rho_t}{\varepsilon_0 \varepsilon_{cloud}} \sum_{n=0}^{N} \frac{\lambda - n\tau}{g} \Phi_n(k_u)\left\{u\left[z-(d+n\tau)\right] - u\left[z-(g+d)\right]\right\} - \frac{\sigma_{PC}(k_u)}{\varepsilon_0 \varepsilon_{PC}} \delta(z-d) \tag{31}$$

where

$$k_u = \sqrt{k_x^2 + k_y^2}, \tag{32}$$

and k_x and k_y are the spatial frequency variables in the x and y directions, respectively. ε_0 is the permittivity of free space, ε_t is the dielectric constant of toner, ε_{pc} is the

$$
\begin{aligned}
E_z(k_u,z) = &-\frac{k_u\cosh(k_u z)}{\sinh\left[k_u(g+d)\right]}\left[V_{bias}\delta(k_u)+\frac{\sigma_{PC}(k_u)}{\varepsilon_0\varepsilon_{PC}k_u}\sinh(k_u g)\right]+\frac{\sigma_{PC}(k_u)}{\varepsilon_0\varepsilon_{PC}}\cosh\left(k_u(z-d)\right)u(z-d)\\
&-\frac{\cosh(k_u z)}{\sinh\left[k_u(g+d)\right]}\frac{\rho_t}{\varepsilon_0\varepsilon_t k_u}\sum_{n=1}^{N}\Lambda_n(k_u)\left\{\begin{matrix}\cosh\left(k_u\left[g-(n-1)\tau\right]\right)\\ -\cosh\left(k_u\left[g-n\tau\right]\right)\end{matrix}\right\}\\
&-\frac{\cosh(k_u z)}{\sinh\left[k_u(g+d)\right]}\frac{\rho_t}{\varepsilon_0\varepsilon_{cloud}k_u}\sum_{n=0}^{N}\frac{\lambda-n\tau}{g}\Phi_n(k_u)\left\{\cosh\left(k_u\left[g-n\tau\right]\right)-1\right\}\\
&+\frac{\rho_t}{\varepsilon_0\varepsilon_t k_u}\sum_{n=1}^{N}\Lambda_n(k_u)\sinh\left(k_u\left[z-(d+(n-1)\tau)\right]\right)u\left[z-(d+(n-1)\tau)\right]\\
&-\frac{\rho_t}{\varepsilon_0\varepsilon_t k_u}\sum_{n=1}^{N}\Lambda_n(k_u)\sinh\left(k_u\left[z-(d+n\tau)\right]\right)u\left[z-(d+n\tau)\right]\\
&+\frac{\rho_t}{\varepsilon_0\varepsilon_{cloud}k_u}\sum_{n=0}^{N}\frac{\lambda-n\tau}{g}\Phi_n(k_u)\sinh\left(k_u\left[z-(d+n\tau)\right]\right)u\left[z-(d+n\tau)\right]\\
&-\frac{\rho_t}{\varepsilon_0\varepsilon_{cloud}k_u}\sum_{n=0}^{N}\frac{\lambda-n\tau}{g}\Phi_n(k_u)\sinh\left(k_u\left[z-(g+d)\right]\right)u\left[z-(g+d)\right]
\end{aligned}
\tag{33}
$$

dielectric constant of the PC and, ε_{cloud} is the dielectric constant of toner cloud, which is assumed to be unity,[18] regardless of the number of developed toner layers. $\sigma_{PC}(x, y)$ is the PC surface charge density, which can be experimentally determined from the photo-induced discharge characteristics (PIDC) associated with the PC. $\Lambda_n(k_u)$, $\Phi_n(k_u)$, and $\sigma_{PC}(k_u)$ are the 2D Fourier transforms of $\Lambda_n(x, y)$, $\Phi_n(x, y)$, and $\sigma_{PC}(x, y)$, respectively. We obtain the potential $V(k_u, z)$ by taking the Laplace transform of Eq. (31) with respect to z, applying the boundary conditions, and then taking the inverse Laplace transform. The normal field is the negative gradient of the potential with respect to z (see Eq. (33)). $\delta(\cdot)$ is the Dirac delta function and V_{bias} is the development bias voltage given by

$$V_{bias} = V_{DC} - V_{AC}\cos\left(2\pi f_{AC}t\right). \tag{34}$$

V_{DC} is the DC developer bias, V_{AC} is the magnitude of the AC bias, and f_{AC} is the frequency of the sinusoidal AC bias. The normal field in the spatial domain is obtained by taking the inverse 2D Fourier transform of Eq. (33).

Development Calculation Procedure

We begin our calculation procedure with the negative peak of the AC bias and the initial gap length g_0 (see Fig. 3). The elapsed time t at this point is therefore zero. Note that it is not necessary to begin with a negative PC rotation angle (see Fig. 6) since the positive peak of the AC bias completely removes any developed toner on the PC when $g = g_0$, as will be shown later. From Eq. (34),

$$V_{bias} = V_{DC} - V_{AC}. \tag{35}$$

Layer-by-layer development is carried out using $g = g_0$ and Eq. (35). We then set $t = 1/(2f_{AC})$, which changes the AC bias polarity. Thus, the developer bias becomes

$$V_{bias} = V_{DC} + V_{AC} \tag{36}$$

During $t = 1/(2f_{AC})$, the PC travels

$$y_{PC}(t) = t\cdot v_{PC}, \tag{37}$$

where v_{PC} is the PC rotation speed, typically specified as a linear velocity, e.g., 10 pages/min. The corresponding PC rotation angle ϕ can be obtained from this PC movement in the y direction

$$\phi = \frac{y_{PC}(t)}{R_{PC}}. \tag{38}$$

The point (x_ϕ, y_ϕ) on the PC in the **z** coordinate system that makes the angle ϕ with the positive x-axis is

$$\begin{aligned} x_\phi &= R_{PC}\cos\phi\\ y_\phi &= R_{PC}\sin\phi. \end{aligned} \tag{39}$$

The corresponding angle θ in the **r** coordinate system is obtained from Eq. (22). We then calculate the effective gap length using θ and Eq. (23). Once the effective gap length and the developer bias, Eq. (36) are determined, we carry out the layer-by-layer development calculation discussed earlier. In the next calculation cycle, we set $t = 1/f_{AC}$ and proceed as before. Note that Λ_n and Φ_n remain the same when we switch from one calculation cycle to the next. They do get modified in the subsequent calculation cycle, but their initial values at the beginning of the current calculation cycle are the same as the final values in the previous calculation cycle.

Simulation Results

We used a 1200 dpi printer with f_{AC} = 2,400 Hz and V_{AC} = 1,050 volts in our simulation. Based on developed toner mass measurements on the test printer, we determined that as many as three toner layers can develop on the PC surface. Consider the bitmap of a vertical line and a 20 × 20 square shown in Fig. 10. Each square in the bitmap represents a printer pixel and our calculation grid spacing is about 2.6 μm. The calculation procedure described in the previous section is implemented in Matlab® and it takes a few minutes on a Pentium® IV machine to complete the calculation procedure for the bitmap in Fig. 10. We first present the results arising from the negative peak of the AC bias. Figure 11 shows

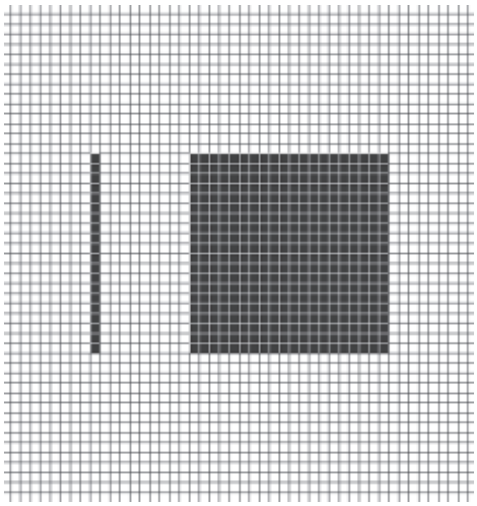

Figure 10. A vertical line and a square

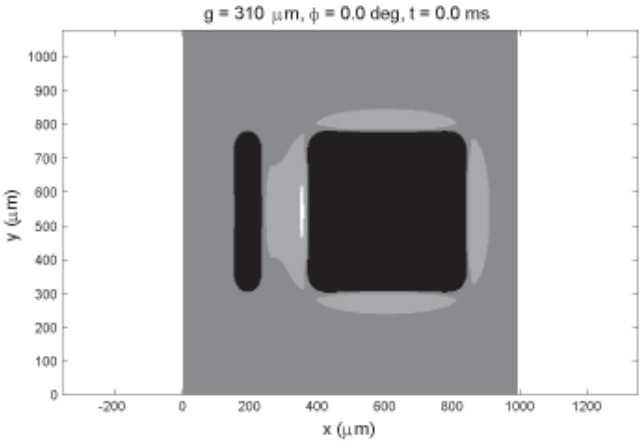

Figure 11. Initial development (negative peak). The number of developed layers is displayed with three grayscales. The lightest gray represents single layer development; the darkest gray (black) represents three layers; the mid tone represents two layers.

the developed toner layers when $g = g_0 = 310$ μm and $t = 0$. The number of developed layers is displayed with three gray levels. The lightest gray represents single layer development; the darkest gray (black) represents three layers; the mid tone represents two layers. Two layers developed on the background, except around the square, where the strong fringe fields prevented the second layer from developing. As the PC rolls away from the developer, the single layer region expands and completely surrounds the square, as shown in Fig. 12 ($t = 40/f_{AC}$). Note that not even a single layer develops in the regions directly adjacent to the four edges of the square. As the PC rotates further away from the developer, no development regions become larger while the regions where two layers developed become smaller, as shown in Fig. 13. Eventually, the two layer regions disappear (Fig. 14). Similarly, the single layer regions become smaller and eventually vanish (Fig. 15 through Fig. 17). It took 200 AC cycles before the background disappears completely. 200 cycles corresponds to a PC rotation angle of 14.82°, effective gap length of 1741 μm. Figure 18 shows the developed layers after 560 AC cycles, which are not much different from the ones after 200 cycles. Thus, one can make an inference that crucial development is completed before the PC rotates about 15 degrees for this test device, after which the amount of toner projecting from the developer to the PC surface is negligibly small, assuming the development field is the dominant force determining the final development.

The positive peak of the AC bias has a tendency to remove developed toner from the PC surface. Thus, the smaller the effect gap length, the less development takes place. In fact, no toner remains on the PC surface if the PC rotation angle is less than 3 degrees, which corresponds to 40.5 AC cycles (t = 16.88 ms). Figure 19 and Fig. 20 show the developed layers after 40.5 and 60.5 cycles, respectively. Note that the corners of the square are getting larger while there is no development on the line. The line begins to develop in the next 10 cycles, as shown in Fig. 21. The second and third layers around the corners of the square begin to appear after 120.5 (Fig. 22) and 170.5 (Fig. 23) cycles, respectively, whereas the second layer on the line does not appear until 170.5 cycles. It seems like the edges of a large pattern begin to develop sooner than for a smaller pattern. On the other hand, the round hole in the middle of the square does

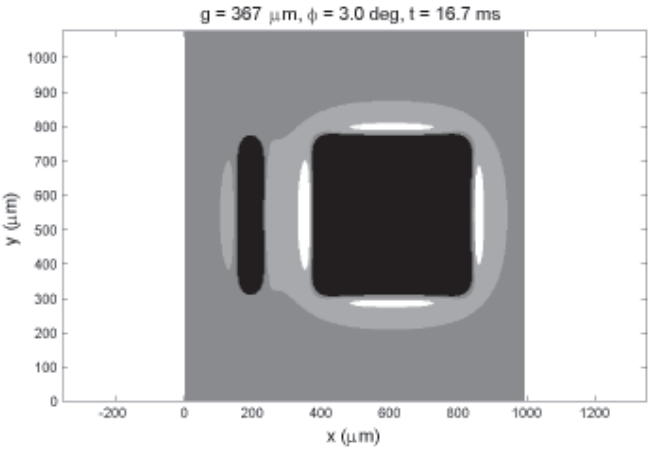

Figure 12. Development after $t = 40/f_{AC}$ (negative peak)

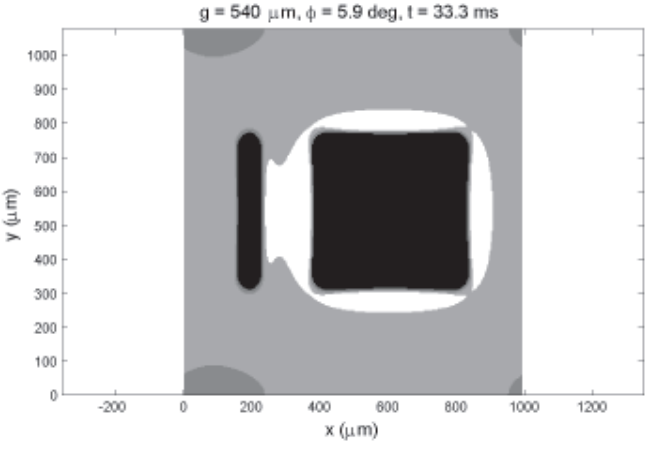

Figure 13. Development after $t = 80/f_{AC}$ (negative peak)

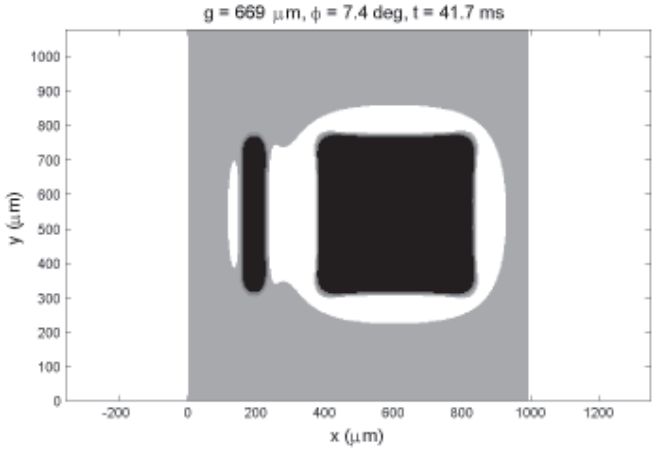

Figure 14. Development after $t = 100/f_{AC}$ (negative peak)

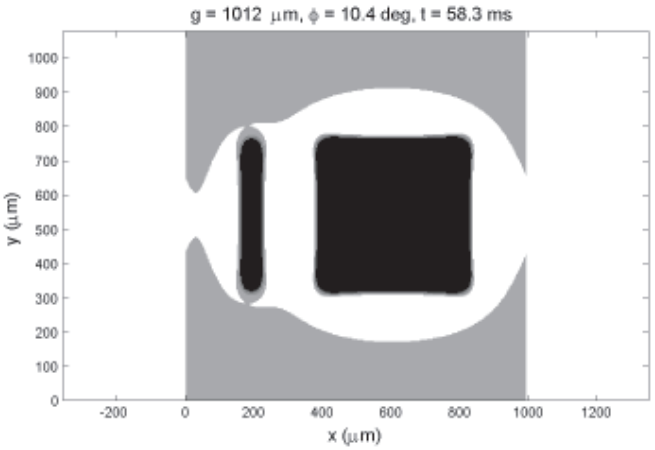

Figure 15. Development after $t = 140/f_{AC}$ (negative peak)

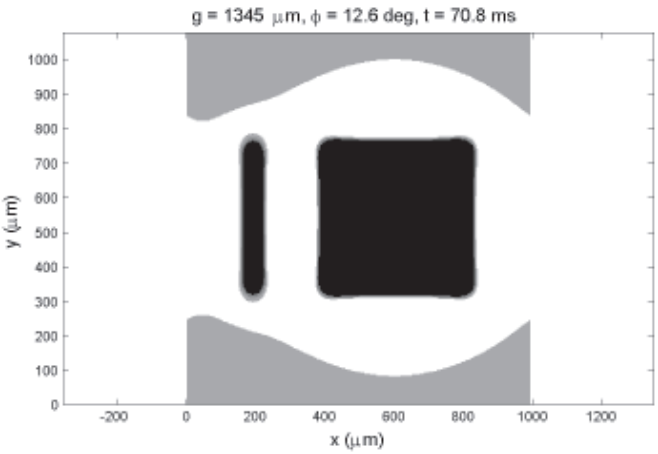

Figure 16. Development after $t = 170/f_{AC}$ (negative peak)

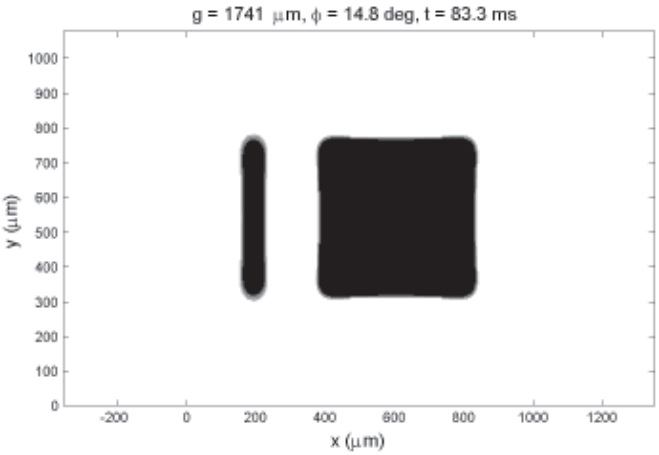

Figure 17. Development after $t = 200/f_{AC}$ (negative peak)

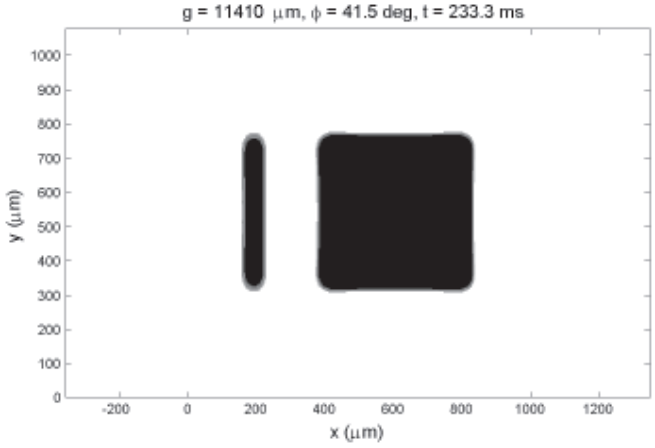

Figure 18. Development after $t = 560/f_{AC}$ (negative peak)

not get filled with the first layer until 200.5 cycles (Fig. 24), at which point the negative peak development more or less completes ($\phi \approx 15°$). It takes another 120 cycles before the second and third layers cover the hole (Fig. 25). Thus, contrary to our earlier speculation, a fair amount of toner does move between the developer and the PC even after the PC rotates about 15 degrees. This can be seen in Fig. 26, where the total developed toner mass from the positive and negative peaks of the AC bias is shown as a function of PC rotation angle. The developed mass from the positive peak continues to increase until the PC rotates about 30 degrees. Also note that the mass from the negative peak does not converge to the same value as that to which the positive peak mass converges. This indicates that at least a small amount of toner keeps moving between the developer and PC even after the developed layers from both peaks stabilize. One can also conclude that a small feature finishes developing earlier than a larger feature since the second layer on the line developed without a gap long before the hole in the square was filled with the second layer. Figure 27 shows the developed layers after 560.5 cycles, which does not look much different from the ones after 320.5 cycles.

A 4 point "*w*" character is shown in Fig. 28. Figure 29 shows the initial development from the negative peak using the "*w*". Relatively light development around the edges of the feature is observed. As in the previous case, the negative peak development stabilizes after the PC rotates about 15 degrees, as shown in Fig. 30. The developed layers from the positive peak, on the other hand, finish developing over a hundred cycles after those from the negative peak stabilize (Fig. 31). Thus, independent of the feature being used, the positive peak keeps the

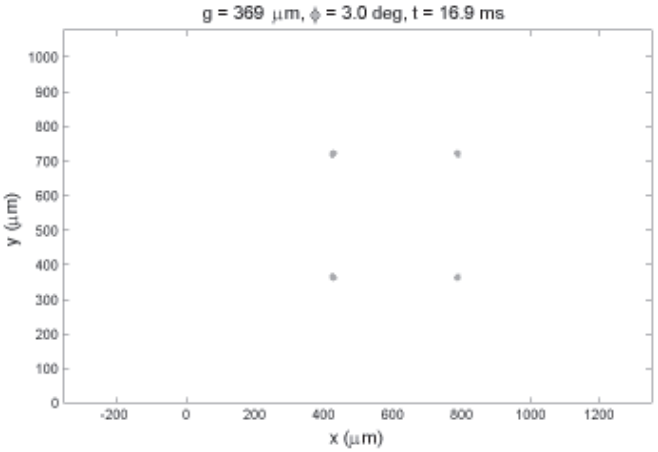

Figure 19. Development after $t = 40.5/f_{AC}$ (positive peak)

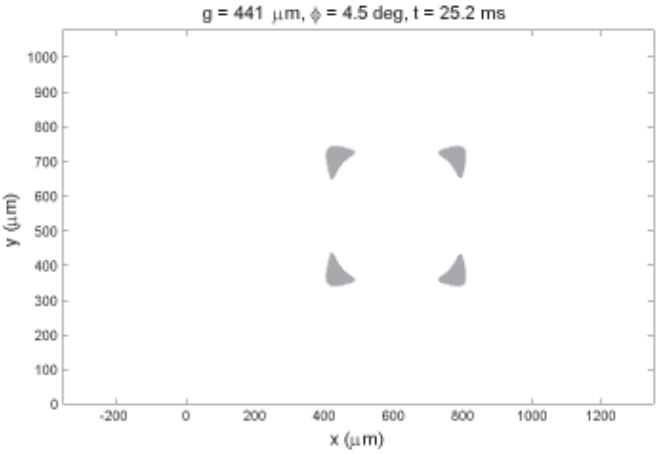

Figure 20. Development after $t = 60.5/f_{AC}$ (positive peak)

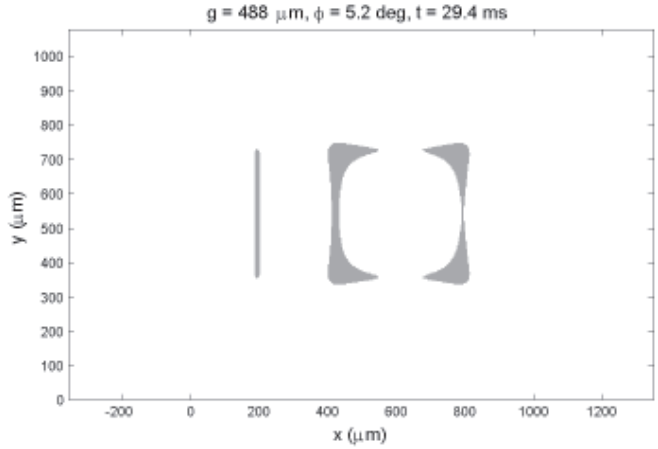

Figure 21. Development after $t = 70.5/f_{AC}$ (positive peak)

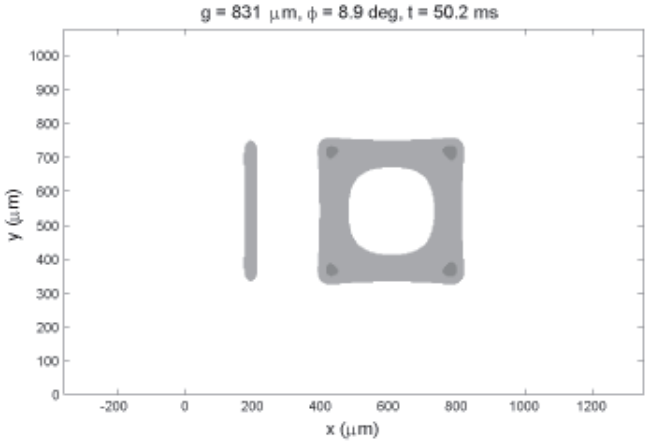

Figure 22. Development after $t = 120.5/f_{AC}$ (positive peak)

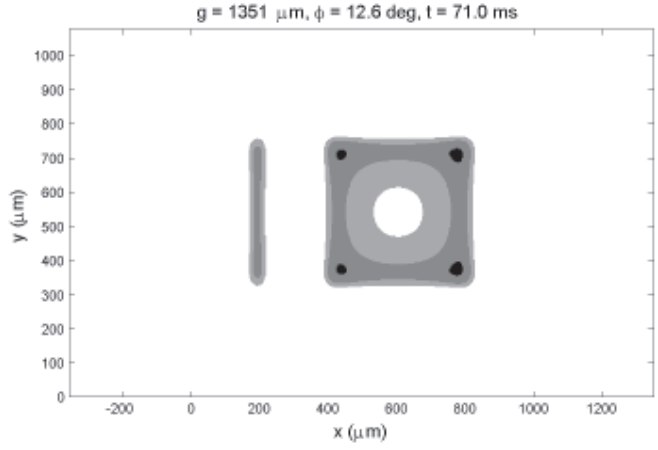

Figure 23. Development after $t = 170.5/f_{AC}$ (positive peak)

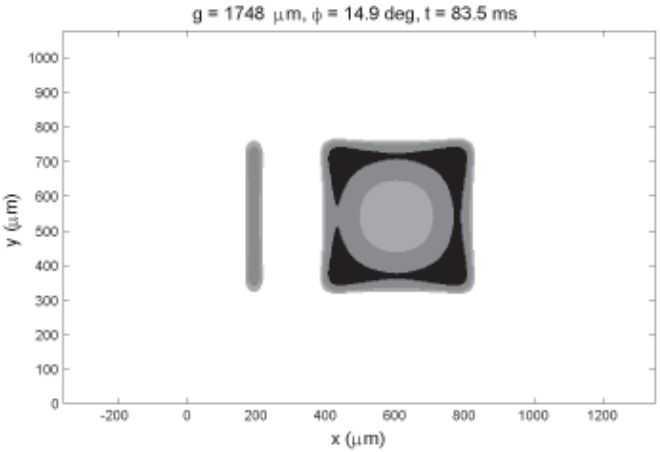

Figure 24. Development after $t = 200.5/f_{AC}$ (positive peak)

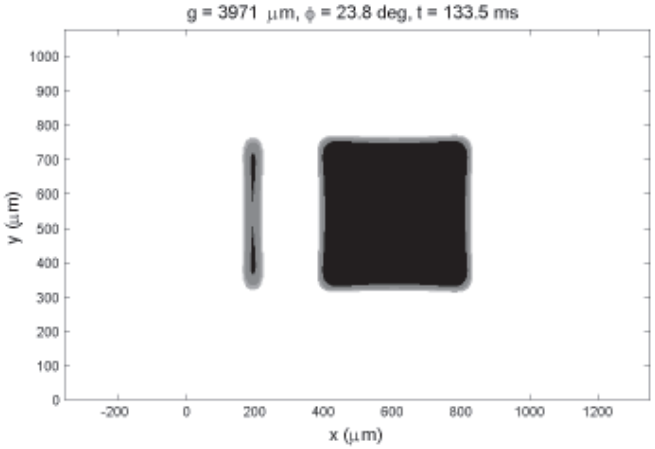

Figure 25. Development after $t = 320.5/f_{AC}$ (positive peak)

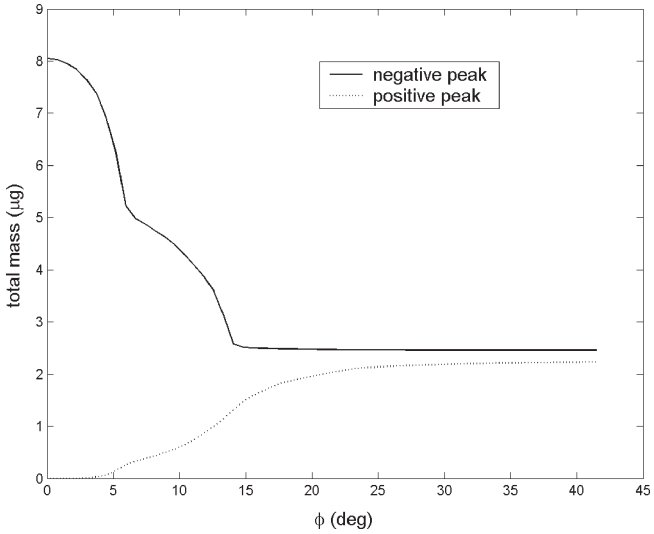

Figure 26. Total developed toner mass

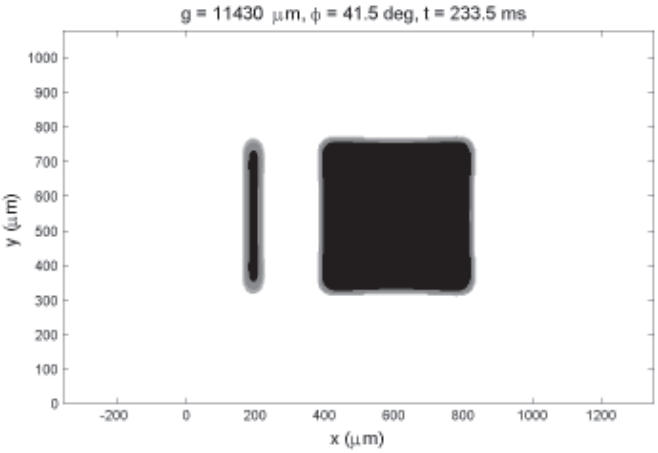

Figure 27. Development after $t = 560.5/f_{AC}$ (positive peak)

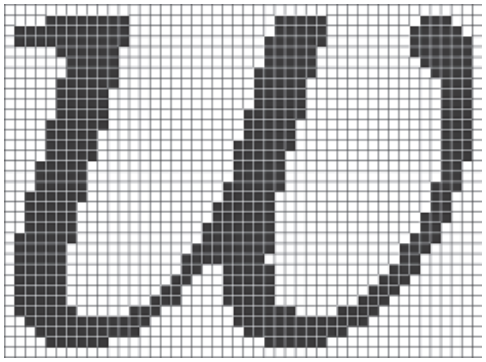

Figure 28. Bitmap of a 4-point "*w*" character

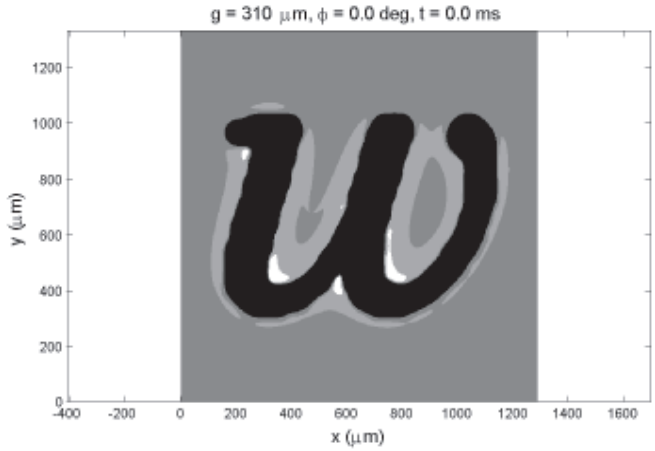

Figure 29. Initial development (negative peak)

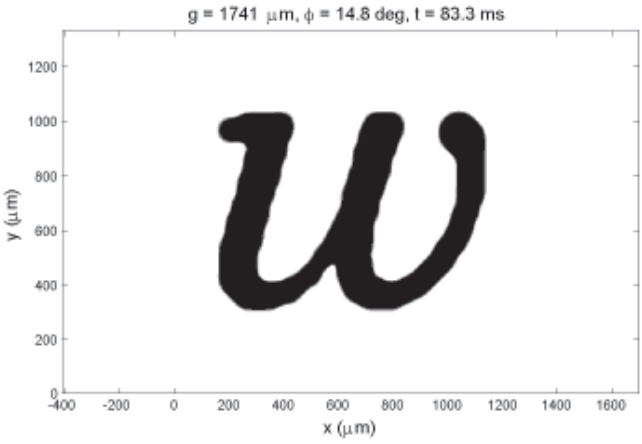

Figure 30. Development after $t = 200/f_{AC}$ (negative peak)

toner particles moving much longer than the negative peak.

Conclusions

Time dependent layer-by-layer development calculation on AC biased monocomponent systems based on uniform toner distribution in the gap was iteratively carried out. The effective gap length as the PC rotates away from the developer was calculated using conformal mapping techniques. The normal electric field in the gap was obtained by talking the 2D Fourier transform of the spatial potential and subsequently taking the negative

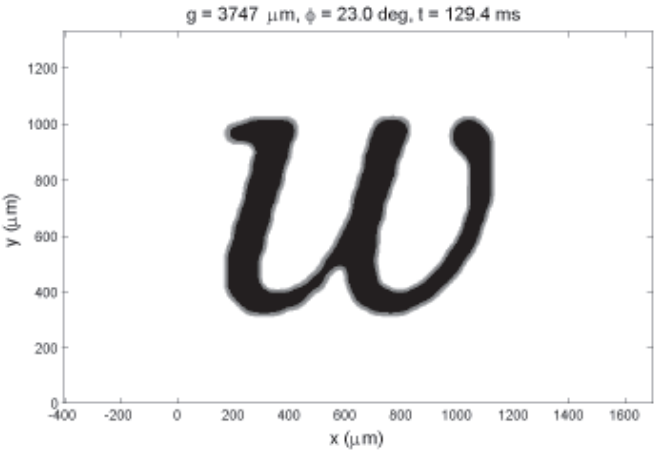

Figure 31. Development after $t = 310.5/f_{AC}$ (positive peak)

gradient of the potential. The field was then used to determine the locations of toner deposition in each toner layer, whose thickness is obtained from the average toner particle size. The negative peak of the AC bias attracts the toner particles towards the PC surface and the positive peak tends to remove the developed toner.

We found that crucial development from the negative peak is completed before the PC rotates about 15 degrees for the test device (f_{AC} = 2,400 Hz and V_{AC} = 1,050 volts). The positive peak, however, continues to remove the developed toner long after the developed layers from the negative peak stabilize. Furthermore, it is found that at least a small amount of toner keeps moving between the developer and PC even after the developed layers from the both peaks stabilize. We also found that a small feature finishes developing sooner than a larger feature (a larger feature tends to form a hole in the middle and it takes longer to cover the hole with toner layers). ▲

Acknowledgment. This research was supported by a grant from Hewlett Packard Company.

References

1. L. B. Schein, *Electrophotography and development physics*, Laplacian Press, Morgan Hill, California, 1992.
2. T. Takahashi, N. Hosono, J. Kanbe, and T. Toyona, Mechanism of Canon toner projection development, *Photogr. Sci. Eng.*, **26,** 254 (1982).
3. T. N. Pappas and D. L. Neuhoff, Printer models and error diffusion, *IEEE Trans. Image Processing* **4,** 66–80 (1995).
4. T. N. Pappas, C. Dong, and D. L. Neuhoff, Measurement of printer parameters for model-based halftoning, *J. Electron. Imaging* **2**(3), 193–204 (1993).
5. F. A. Baqai and J. P. Allebach, Printer models and the direct binary search algorithm, *Proc. 1998 IEEE International Conference on Acoustics, Speech, and Signal Processing*, vol. 5, IEEE, Los Alamitos, CA, 1998, pp. 2949–2952.
6. C. J. Rosenberg, Measurement based verification of an electrophotographic printer dot model for halftone algorithm tone correction, *Proc. IS&T's 8th Int'l. Cong. Adv. Non-impact Printing*, IS&T, Springfield, VA, 1992, pp. 286–291.
7. R. Hendriks, Simulation of the development process in electrophotography, *Proc. IEEE Industry Applications Society Annual Meeting*, IEEE, Los Alamitos, CA**,** 1989, pp. 2248–2255.
8. L. B. Schein, Electric field enhancement in the magnetic brush developer, *Photogr. Sci. Eng.* **19**(1) (1975).
9. J. Yi, R. B. Wells, and T. Camis, Gray level and DMA estimation in monocomponent development systems, *Proc. NIP-18 Int'l. Conference on Digital Printing Technologies*, IS&T, Springfield, VA, 2002, pp. 726–731.
10. T. Teshigawara, H. Tachibana, and K. Terao, Simulation of toner depositing process in xerographic image studies, *IEEE Trans. Industry Appl.* **24**(2), 232–237 (1988).
11. E. M. Williams, Electrostatic field of arctangent voltage transitions in electrophographic images, *Photogr. Sci. Eng.* **26**(2), 88–91 (1982).
12. H. E. J. Neugebauer, Electrostatic fields in xerography, *Appl. Opt.* **3**(3) 385–39 (1964).
13. C. C. Kao, Electric field, transfer, and spread functions in xerographic image studies, *J. Appl. Phys.* **44**(4) 1543–1551 (1973).
14. J. Yi, R. B. Wells and T. Camis, Electric field calculation based on PIDC in monocomponent development systems, *Proc. IS&T's NIP18: Int'l. Conference on Digital Printing Technologies*, IS&T, Springfield, VA, 2002, pp. 23–27.
15. M. H. Lean, Simulation and visualization of 3D particle cloud electrodynamics, *IEEE Trans. Magnetics* **28**(2), 1271–1274 (1992).
16. J. G. Shaw, T. Retzlaff and S. Ramesh, Particle based simulations of image quality defects, *Proc. IS&T's 50th Annual Conference*, IS&T, Springfield, VA, 1997, pp. 269–272.
17. J. H. Mathews and R. W. Howell, *Complex Analysis for Mathematics and Engineering*, Jones and Bartlett, Sudbury, MA, 1997, pp. 343.
18. D. Stroud, The effective medium approximations: some recent developments, *Superlattices and Microstructures* **23**(3/4) 1998.